CONF-890663--17

SAND--89-1458C

DE89 014782

PBFA II APPLIED B-FIELD ION DIODE PROTON BEAM CHARACTERISTICS*

D. J. Johnson, T. R. Lockner, R. J. Leeper, J. E. Maenchen, C. W. Mendel, G. E. Rochau, W. A. Stygar, R. S. Coats, M. P. Desjarlais, R. P. Kensek, T. A. Mehlhorn, W. E. Nelson, S. E. Rosenthal, J. P. Quintenz, and R. W. Stinnett

Sandia National Laboratories, Albuquerque, NM 87185

Abstract

An applied B-field ion diode on PBFA II has produced a 17 TW proton beam for investigation of beam generation and transport physics pertinent to inertial confinement fusion experiments. Power was fed to the diode via two conical self-magnetically-insulated transmission lines that incorporated plasma opening switches. The diode utilized a pair of B-field coils in disc shaped cathodes to produce a 3 T axial B-field that insulated the 16 mm anode-cathode gap from electron loss. The 15-cm-radius anode was configured with a 5.5-cm-tall curved ion emitting region. A 2.6 MA ion beam originated from this region, was accelerated to 6 MV in the anode-cathode gap, and then transported ballistically toward the axis in a current neutralizing gas cell. The best transport (75%) occurred with narrow 5.5-cm-tall anode sources in which a 180 kJ proton beam was observed within 1.2 cm of the diode centerline. The FWHM of the beam focused at the centerline of the diode was 5 to 7 $_2$mm. This beam gave a peak proton power density of approximately 5 TW/cm^2.

I. Introduction

An ion diode is being developed at Sandia National Laboratories for ion beam driven inertial confinement fusion experiments with the PBFA II accelerator[1]. A cross sectional view of the diode is shown in Fig. 1. This diode is a scale-up of a smaller diode[2] used previously on the Proto I accelerator. Two cathode coils supply the primary insulating B-field in the anode-cathode (AK) gap but work in concert with four anode coils to produce uniform magnetic insulation along the anode surface to give a proton beam with zero canonical angular momentum. The anode source operates by surface flashover and is a series of concentric grooves machined in stainless steel, 0.9 mm wide, 1.5 mm deep, separated by a 0.3 mm land, and filled with wax. Electron loss early in the diode power pulse creates an anode plasma on the wax. This plasma is a mix of ions and neutrals that give rise to beam energy spread, and yields a beam with comparable currents of proton and carbon ions. The thickness of this plasma necessitated placing the zero stream function (separatrix) of the applied B-field about 3 mm from the anode surface to give a zero canonical angular momentum beam.

When the PBFA II power pulse is applied to the 18.5 Ω self-magnetically-insulated transmission lines (MITL), a spiral gun array, plasma opening switch (POS) shunts the leading edge of the current pulse. The POS consists of two arrays of four guns, each with 25 cm^2 aperture, located 20 cm above and below the diode. When the POS opens, the rising voltage pulse allows electrons to flow into the diode to fill the AK gap and form a virtual cathode of azimuthally drifting electrons. This enhances the ion flow about a factor of 10 over the normal space-charge limited value at peak power but results in a beam turn-on delay with respect to the voltage of

---

about 5 ns . The beam is then accelerated by the applied electric field in a distance of about a third of the AK gap because of the compression of the equipotentals towards the anode surface. During ballistic transport to the centerline of the diode the beam undergoes self and applied B-field bending. At 12.5-cm-radius, it enters a gas cell with 2-μm-thick Mylar window and 5-Torr-argon fill, that allows current neutralization and reduces the self field bending by a factor of about 10. The applied field bending varies as B^2 and roughly as the square of the distance from the midplane and is not affected by the gas cell. For this reason the anodes had a complex shape to allow a good focus at the centerline. Typical proton trajectories for a 6 MV, 2.6 MA proton beam obtained with the simulation program PICDIAG[3] are shown in Fig. 2 along with the applied B-field lines calculated with the magnetic diffusion program TRIDIF[4]. The protons were emitted normal to anode shape Q1 described below (Fig. 5) and the beam assumed to be 90% current neutralized in the gas cell.

II. Diagnostics

The total and ion currents were measured with dB/dt loops on the negative transmission line feeds before and after the POS and near the edges of the cathodes at 13 cm radius, respectively. The diode voltage was determined two ways. First, using an array of six range-filtered scintillator fiber-optics channels (RFS Monitor in Fig. 1) observing protons from a 6 cm^2 flashover source in the bottom transmission line. An LdI/dt correction was made in this case for the 20 nH inductance between the monitor and diode positions. Second, the diode voltage was specified by an LdI/dt correction to the voltage measured across the vacuum insulator stack. This measurement was only accurate after peak power when full self magnetic insulation was established in the vacuum transmission lines.

The beam was measured with full beam and shadowbox witness plates, K_α and Rutherford-scattering pinhole cameras, and a magnetic spectrometer. The shadowbox consisted of an aperture plate at the gas cell window with an array of 35 holes, 1.5 mm diameter, used in conjunction with a witness plate at 7 cm radius. Three additional 90° sectors of the beam[5] were observed at 3.8 cm radius with time-integrated K_α pinhole cameras. One camera recorded the total incoming beam, a second the beam transmitted through a slotted mask at the gas cell window, and a third after it passed through a gold foil at the centerline.

The proton beam energy spectrum and focused power density were measured with a time-resolved magnetic spectrometer[6] that observed protons Rutherford scattered from a 0.1-μm-thick gold foil located at the center of the diode as shown in Fig. 1. The spectrometer utilized 250-μm-thick PIN diodes and CR39 track recording film to observe the beam. A 1-mm-diameter aperture at the entrance to the spectrometer acted with a 3-mm-wide slit mounted 3.8 cm above the target to give an energy-resolved ($\delta E/E \sim 1.5\%$) one dimensional image of the beam in the horizontal plane. The spatially-resolved energy density of the focused beam was observed also at the on-axis gold foil with an array of six range-filtered Rutherford scattering ion pinhole cameras.[7] Since the Rutherford scattering cross section varies as $\sin(\theta)^{-4}$ with scattering angle θ and the effective target thickness varied with incident beam angle, the scattering probability was most uniform with angle for the transmission geometry target. This fact mandated separate shots to acquire accurate data on both the spectrometer and pinhole camera. The filters gave

energy discrimination and since the diode voltage dropped throughout the pulse this implicitly yielded a time resolved focus.

III. Experimental

A. Beam generation

The electrical characteristics of diode shot 2679 are shown in Fig. 3. This shot utilized an applied B-field that varied across the anode surface from 2.2 T at the midplane to 3.2 T at the AK gap and gave a TRIDIF calculated V_{crit} of 12.8 ± .05 MV across the 5.5-cm-tall anode emitting region. The first 35 ns of the voltage pulse was obtained with the RFS monitor and the remainder with the inductively corrected monitor. The diode current rises before the ion current because of electrons conducted into the diode along the applied B-field lines prior to the formation of the virtual cathode.[8] After the establishment of the virtual cathode, experiment[9,10] and theory[9,10] demonstrate the existence of a limiting voltage at which the ion current diverges. This limiting voltage, $V_* \sim 0.6cB_o d$, is proportional to the flux ($B_o d$) in the AK gap. The heavy dashed line in Fig. 3 shows the result of a time dependent calculation of the voltage decay caused by a flux loss behind the active anode surface.[10] The initial starting voltage is the theoretical operating-point voltage determined from the steady-state theory. The time-dependent part of the calculation contains one free parameter characterizing the anode plasma motion.

The currents obtained upstream and downstream from the POS, I_{feed} and I_{diode}, respectively, indicate that about 1.0 MA of current was conducted by the POS. When open, the POS operated like a 10 Ω MITL and absorbed power until the diode impedance dropped below about 5 ohm. The diode power pulse showed a factor of two increase in rise rate and was 10% higher at peak with use of this POS. Three shots were fired with a dual flashboard plasma source POS that utilized six 75 cm^2 apertures above and below the diode. This arrangement gave a much later opening time, and resulted in POS action that was approximated by a 5 Ω MITL. In this case the POS intercepted energy until the diode impedance dropped to 2 Ω.

Data were obtained first with various height flat anodes. The narrow anodes gave a longer beam turn-on delay, more voltage overshoot, more rapid impedance collapse, and less energy coupled to the diode. These effects are attributed to the requirement for a smaller dynamic gap in this case that accentuates the effects of anode plasma motion. For a 5.5-cm-tall anode about 650 kJ of electrical energy was coupled to the diode with 450 kJ in ions. This increased to 750 and 600 kJ, respectively, for an 8-cm-tall anode. However, tall anodes produced proton beams that were very susceptible to applied B-field bending near the coils. For a 5.5-cm-tall anode, 180 kJ of proton beam energy was observed within 1.2 cm of the diode center. This dropped to 85 kJ when the anode height was increased to 8.5 cm. A simulation of the beam transported to the target region with PICDIAG, assuming half the beam current was protonic and the remainder carbon, agreed with these experimental values to within 20%.

Other criteria for successful diode operation were magnetic insulation uniformity (conformity of the B-field lines to the anode surface), B-field strength, size of the AK gap, and position of the gas cell. Decreasing the magnetic insulation in a region of the anode resulted in higher current

density. For this reason it was necessary to use less insulation at the midplane of the anode to compensate for the tendency for lower current density there, if uniform current density was desired. Larger B-fields and AK gaps gave longer beam turn-on delays and a larger focus FWHM. The reason for this is not fully understood. However, a nonuniform anode plasma could occur during the longer turn-on associated with the large gaps thereby giving an poorer focus. Another possibility is that the shorter cathode tips used with large gaps could result in a virtual cathode being formed by electrons from the feed region near the diode or gas cell.

B. Proton Focus

The rear surface spall on a 1.6-mm-thick stainless steel shadowbox aperture plate exposed to the beam from a 6.5-cm-tall flat anode is shown in Fig. 4. The spall shows well defined top and bottom edges that are azimuthally symmetric in axially position to ± 1 mm and located where predicted with PICDIAG for the peak power beam. A representation of the proton beam produced shadowbox damage patterns obtained for anode Q1 (shot 2646) is shown in Fig. 5 along with a plot of the anode slope. The patterns represent front surface blow-off on a brass witness plate and were typically 2 mm wide. These imply an intrinsic divergence of 13 mr and would give a 3.8-mm-FWHM focus. The data also show that the beamlets are randomly scattered within 1 mm of their desired positions. This indicates a global divergence of 20 mr that is sufficient to produce the 5.5-mm-FWHM focus observed on this shot. The projections of the beamlets allowing for self and applied B-field bending of the beam are also shown in Fig. 5. The 6-cm-tall anode used on this shot resulted in a 10% lower diode impedance than observed for shot 2679, therefore the applied B-field bending was greater.

The open quadrant Ti cone target K_α pinhole camera image for shot 2646 is represented in Fig. 6 by the projection of the image on a 3.8-cm-radius cylinder. A similar projection based upon a time integrated PICDIAG simulation for the beam is also shown in Fig. 6. The simulation used the beam energy determined from the magnetic spectrometer and beam current from the ion dB/dt loops. Small angle scattering in the gas cell window and gas was included and current neutralization inside the gas cell taken to be 90%. It assumed normal emission from the anode surface Q1 and a histogram current density function that increased by two above the nominal value at axial distances of between 33 and 66% of the anode half height. This gave a better PICDIAG fit to masked K_α camera images than uniform current density. This current density enhancement at half anode height was difficult to discern from the shadowbox witness plate damage patterns because of the sweeping of the beamlets above and below the miplane.

A comparison of the experimental and theoretical data in Fig. 6 shows that azimuthal non-uniformities of the beam at 3.8 cm radius are ± 40%. Similar analysis of the images of the beam projected through a 6-mm-wide slot at the gas cell window show a ± 25% variation. Non-uniformities in current density at the anode result in local applied electric and self magnetic focusing[11] of the beam during transport and contribute to the non-uniformities at the K_α target. A current density variation of ± 20% in this diode would give magnetic steering errors of 1° and increase current density variations on the K_α target by at least 10%, in agreement with these measurements. The most intense region of the beam appears to oscillate up and down in a serpentine pattern in Fig. 6. This indicates that the virtual

cathode sheath is not symmetric in the azimuthal direction, implying asymmetrical power flow or unstable virtual cathode development.

The images in Fig. 7 were obtained with the Rutherford scattering pinhole camera array on shot 2646 and show the focus of a 67° sector of the proton beam on the gold foil at the center of the diode. The horizontal FWHM of the focus increased from 5.5 mm at beam energies above 6.5 MeV to 7 mm at beam energies between 4.0 and 3.6 MeV. The vertical profile of the beam shows the effects of magnetic sweeping. The best vertical focus of 4.9 mm FWHM occurred in the 5.7 to 5.1 MeV energy interval. Similar results were obtained for shot 2679 except that the target was mounted in the reflection geometry for the pinhole camera giving an asymmtrical profile as expected due to the variation in scattering sensitivity with beam angle. The horizontal FWHM for shot 2679 was 5 mm for the high energy portion of the beam.

The PIN diode signals and CR39 image from the magnetic spectrometer are shown in Fig. 8, along with an unfold of the beam power for a 67° sector, based upon computer generated response curves for the spectrometer. The beam is observed to have an energy spread of ± 5% throughout the power pulse. The beam energy is also plotted in Fig. 2 where it appears to be 20 and 10% below the diode voltage early and late in the pulse, respectively. This may be due to a charge exchange mechanism[12] in a weakly ionized anode plasma penetrated by the applied electric field. In the charge exchange process, an accelerated ion captures an electron from a slow neutral atom resulting in a fast neutral and a new ion at somewhat less that the total gap potential. In this manner the final ion energy is less than that for full gap acceleration.

The focused proton beam power shown in Fig. 8 was determined from the PIN signals for the 67° beam sector striking the gold foil target and converted to power on a vertical planar target. Energy and temporal integration of the CR39 tracks and PIN signals gave energy densities of 73 and 67 kJ/cm^2 on the target, respectively, above 5 MeV. These energy densities are consistent with data obtained with the Rutherford scattering pinhole camera array that showed a target energy density of 63 kJ/cm^2, above 5.1 MeV. The peak power density of 4.8 TW/cm^2 determined from the PIN signals is consistent also with a forward simulation of the beam focus with PICDIAG that gives 5.3 TW/cm^2. The measured value, projected to equivalent power density deliverable to a 6-mm-diameter spherical target, the baseline for PBFA II, is 5.4 ± 0.9 TW/cm^2.

*This work was supported by the U. S. Department of Energy under Contract DE-AC04-76-DP00789

References

1. D. L. Cook, M. P. Desjarlais, S. A. Slutz, T. R. Lockner, D. J. Johnson, S. E. Rosenthal, J. E. Bailey, R. S. Coats, R. J. Leeper, J. E. Maenchen, T. A. Mehlhorn, T. D. Pointon, J. P. VanDevender, in "Proceedings of the 7th International Conference on High-Power Particle Beams", edited by W. Bauer and W. Schmidt, (Kernforschungszentrum Karlsruhe GmbH, Karlsruhe, Germany, 1988), p 35.

2. D. J. Johnson, R. J. Leeper, W. A. Stygar, R. S. Coats, T. A. Mehlhorn, J. P. Quintenz, S. A. Slutz, and M. A. Sweeney, J. Appl. Phys. 58, 12 (1985).
3. T. A. Mehlhorn, W. E. Nelson, J. E. Maenchen, W. A. Stygar, E. L. Ruiz, T. R. Lockner, and D. J. Johnson, Rev. Sci. Instrum. 59, 1709 (1988).
4. J. R. Freeman, J. Comput. Phys. 41, 142 (1981).
5. J. E. Maenchen, T. A. Mehlhorn, D. F. Wenger, R. J. Leeper, D. J. Johnson, and T. R. Lockner, Rev. Sci. Instrum. 59, 1706 (1988).
6. R. J. Leeper, W. A. Stygar, R. P. Kensek, J. R. Lee, D. J. Johnson, T. R. Lockner, J. E. Maenchen, D. E. Hebron, and D. F. Wenger, Rev. Sci. Instrum. 59, 1700 (1988).
7. W. A. Stygar, R. J. Leeper, L. P. Mix, E. R. Brock, J. E. Bailey, D. E. Hebron, D. J. Johnson, T. R. Lockner, J. Maenchen, T. A. Mehlhorn, and P. Reyes, Rev. Sci. Instrum. 59, 1703 (1988).
8. P. M. Miller, J. Appl. Phys. 57, 1473 (1985).
9. M. P. Desjarlais, Phys, Rev. Lett. 59, 2295 (1987).
10. M. P. Desjarlais, Submitted to Phys. Fluids B.
11. D. J. Johnson, P. L. Drieke, S. A. Slutz, R. J. Leeper, E. J. T. Burns, J. R. Freeman, T. A. Mehlhorn, and J. P. Quintenz, J. Appl. Phys. 54, 2230 (1983).
12. T. D. Pointon, submitted to J. Appl. Phys., M. P. Desjarlais, submitted to J. Appl. Phys.

Figure Captions

Fig. 1. Cross sectional view of the diode showing the diagnostics layout.

Fig. 2. Trajectories calculated with PICDIAG for a 6 MeV, 2.6 MA proton beam. (Upper) Trajectories in the horizontal plane where $X = R \times \mathrm{Cos}(\theta)$ and $Y = R \times \mathrm{Sin}(\theta)$. (Lower) Trajectories in the vertical plane and applied B-field lines calculated with TRIDIF displayed on a schematic of the diode.

Fig. 3. Electrical characteristics of the diode.

Fig. 4. Rear surface spall pattern for a 9.5-cm-tall shadowbox aperture plate.

Fig. 5. (Upper left) Shadowbox beamlet damage patterns. (Upper right) Slope of anode Q1 versus axial position. (Bottom) Ion trajectories projected on a schematic of the diode.

Fig. 6. (Left) The K_α camera image observed from the open quadrant on shot 2646. The peak intensity is divided into 15 contour levels. (Right) The K_α image calculated for this geometry with the PICDIAG computer code. The peak intensity is divided into 9 contour levels. The non-uniformities represent 25 fiducial holes located in the Ti target to identify possible target motion caused by the applied B-field.

Fig. 7. Rutherford scattering pinhole camera images for shot 2646 displayed as a function of beam energy. The peak current density for the 6.5 -5.7 MeV image is 21 kJ/cm^2. The contour levels show equal beam charge density on target and energy densities of $0.65 \times E(MeV)$ $kJ/(cm^2 MeV)$.

Fig. 8. (Upper left) Proton focus power for shot 2679. (Upper right) Raw PIN diode data from the magnetic spectrometer. The largest signal corresponds to ions at 5.9 MeV. (Lower) The image of the beam as recorded by the CR39 in the magnetic spectrometer. The image is blocked at several locations by 2-mm-diameter holes in the CR39 to allow ions into the PIN's.

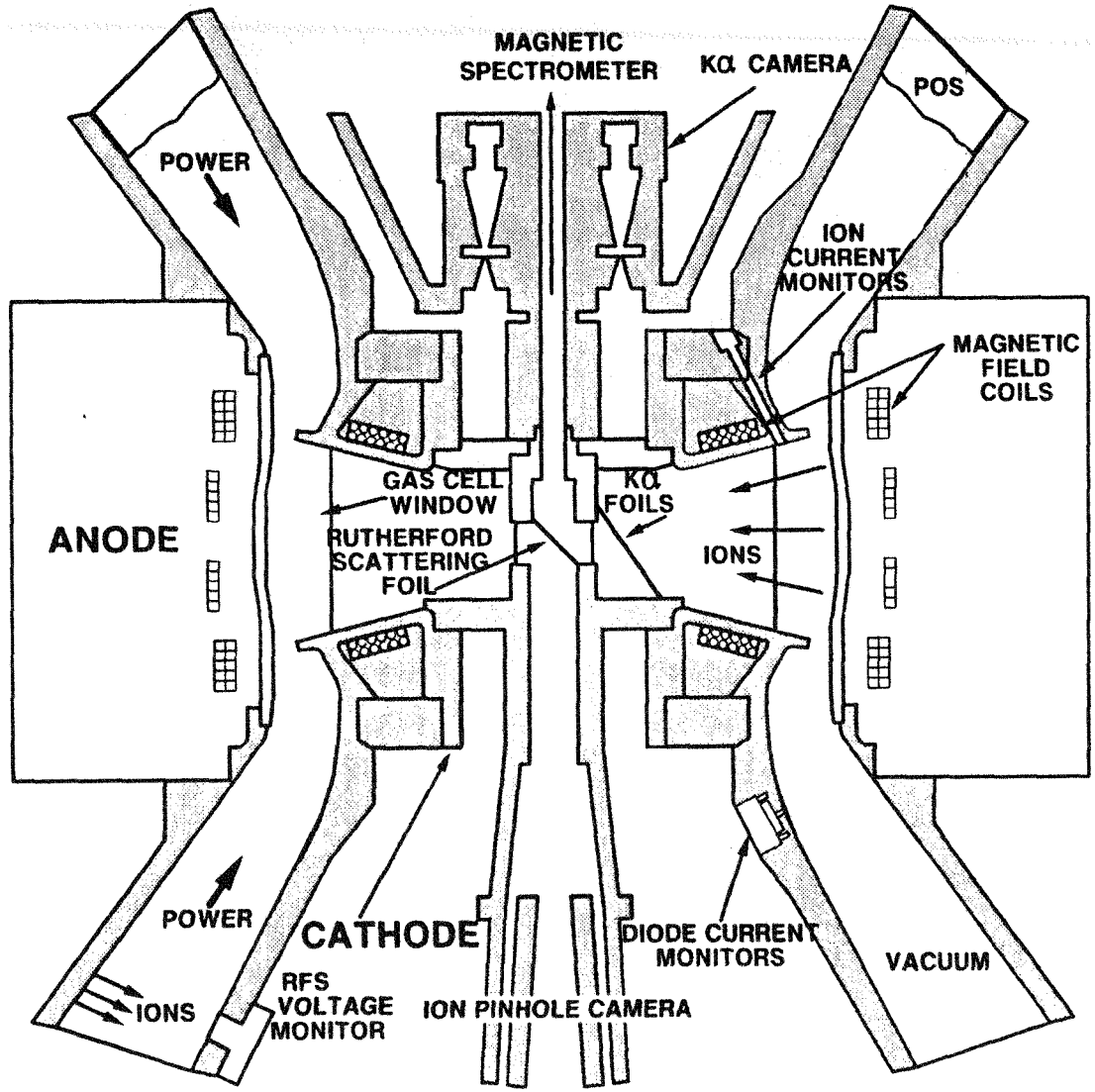

89L1000.35

Sandia National Laboratories

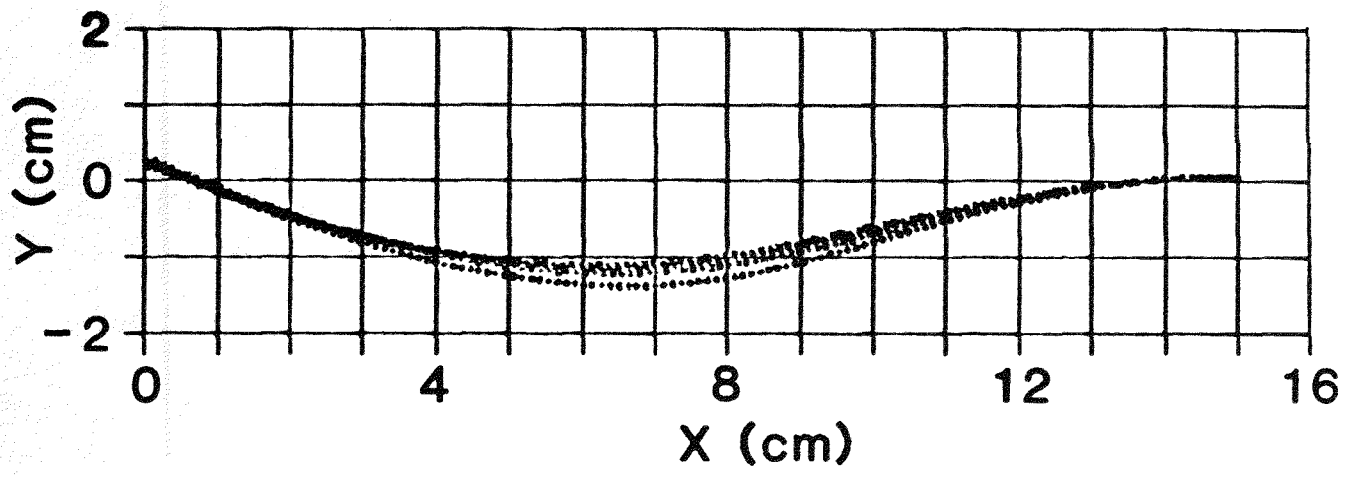
2
0
-2
Y (cm)
0
4
8
12
16
X (cm)

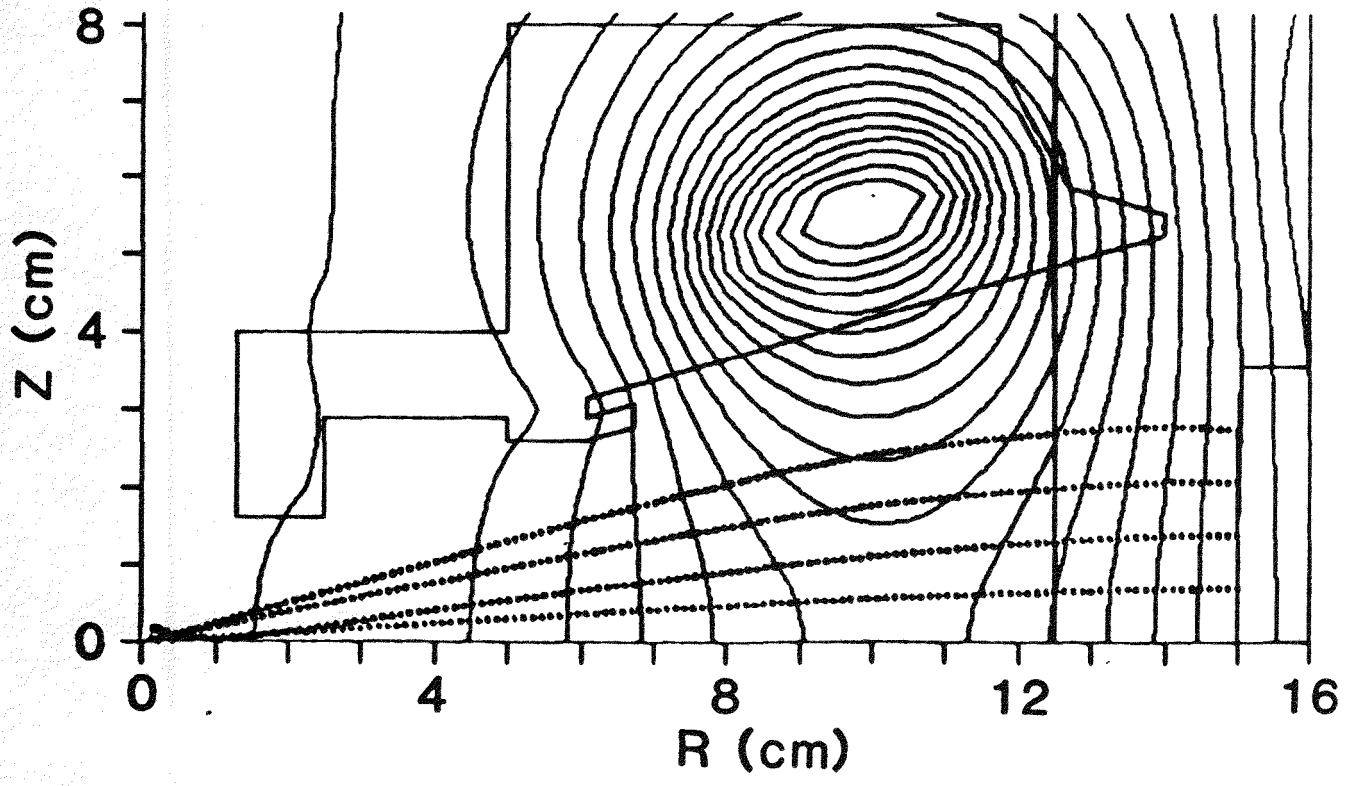
8
4
0
Z (cm)
0
4
8
12
16
R (cm)

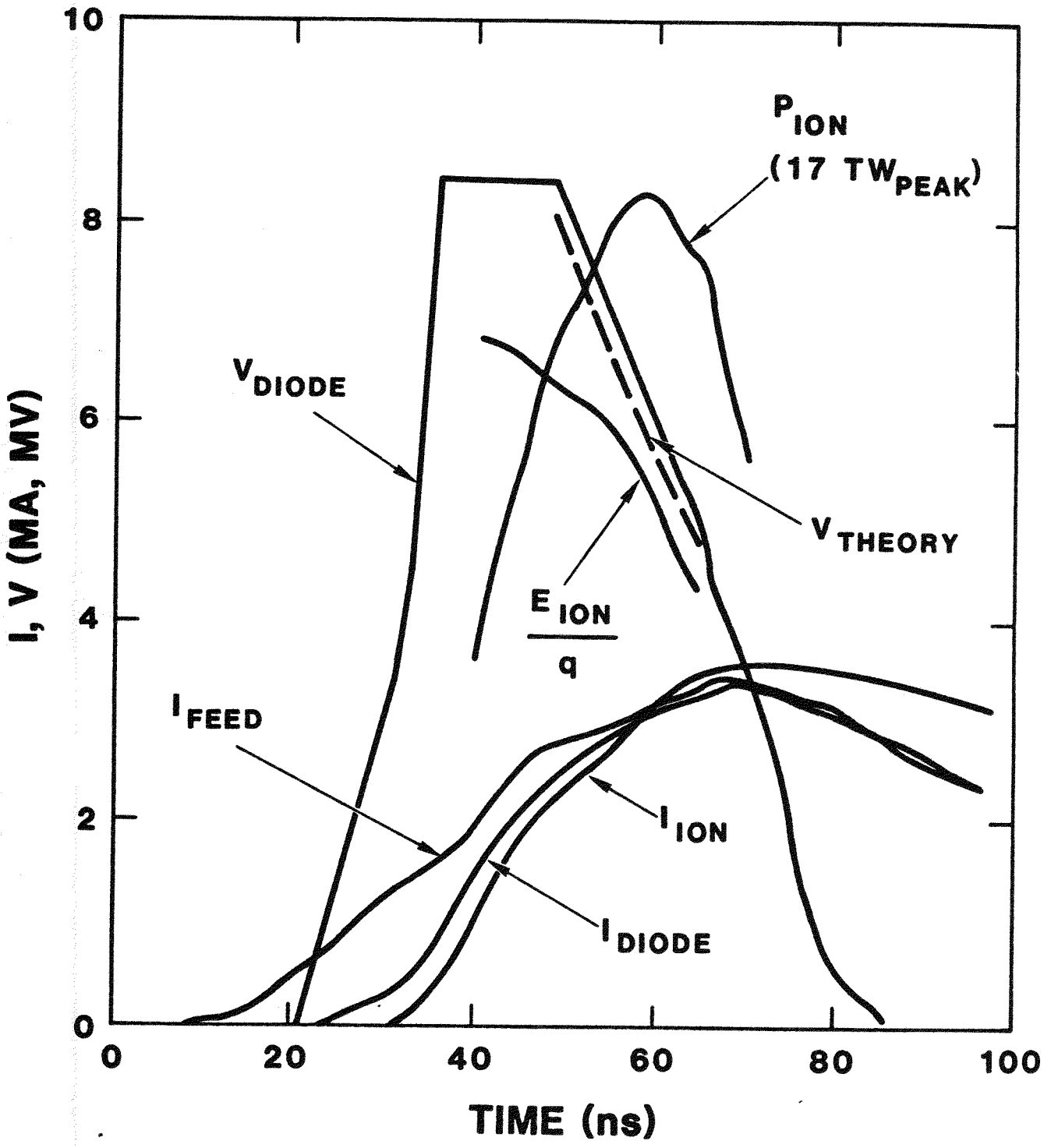
10
8
6
4
2
0
0
20
40
60
80
100
I, V (MA, MV)
TIME (ns)
P ION
(17 TW PEAK)
V DIODE
V THEORY
E ION
q
I FEED
I ION
I DIODE

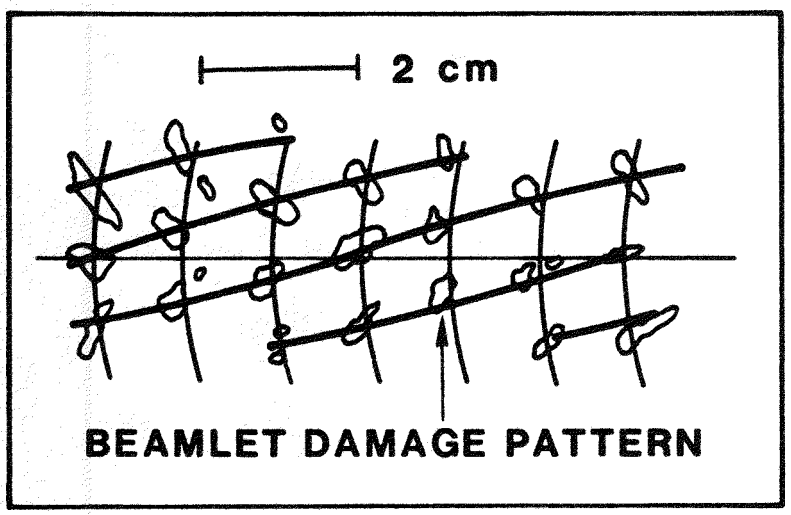
2 cm
BEAMLET DAMAGE PATTERN

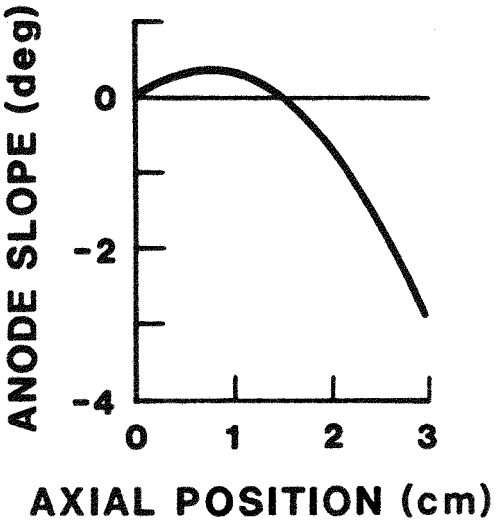
ANODE SLOPE (deg)
0
-2
-4
0
1
2
3
AXIAL POSITION (cm)

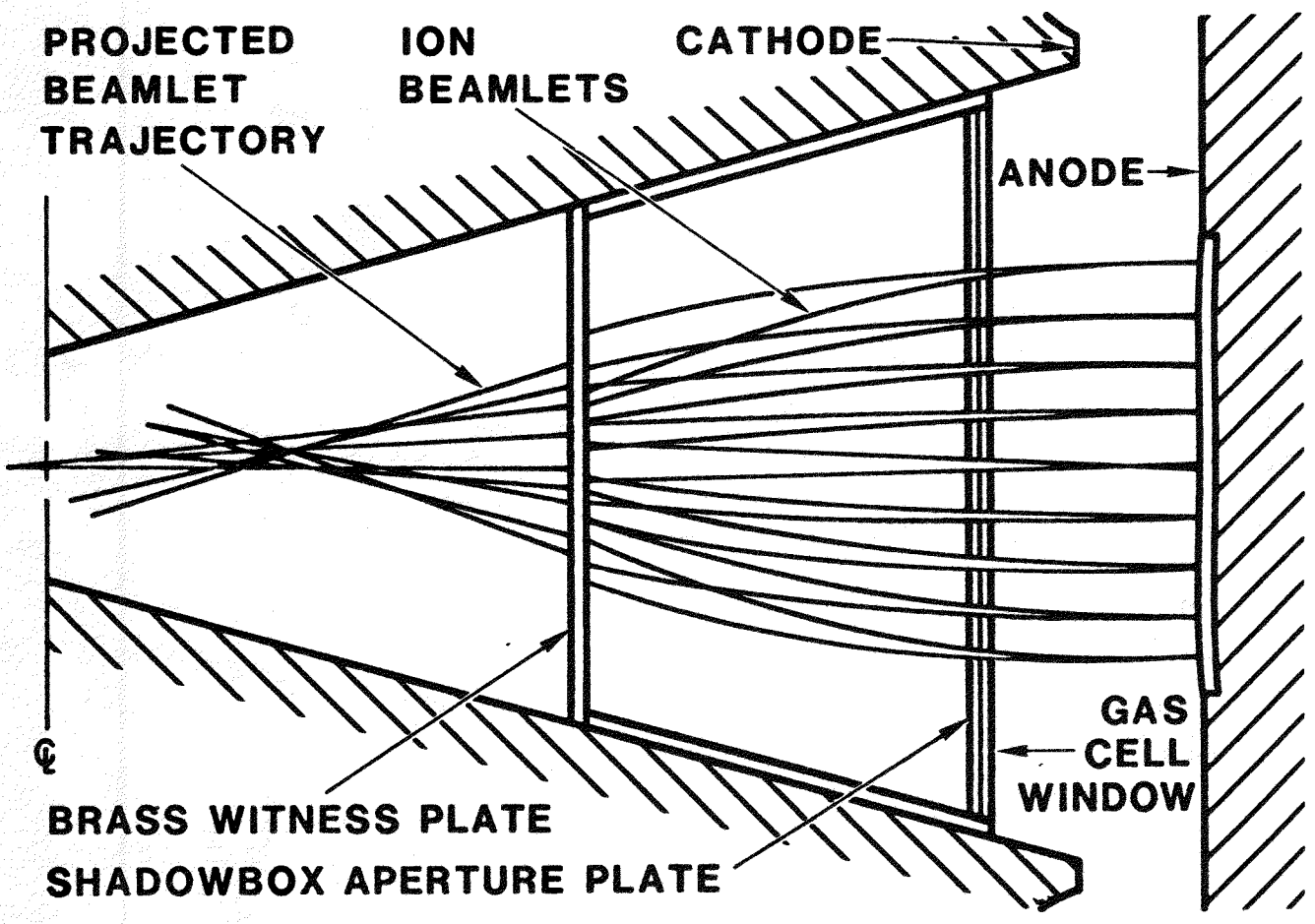
PROJECTED BEAMLET TRAJECTORY
ION BEAMLETS
CATHODE
ANODE
GAS CELL WINDOW
BRASS WITNESS PLATE
SHADOWBOX APERTURE PLATE

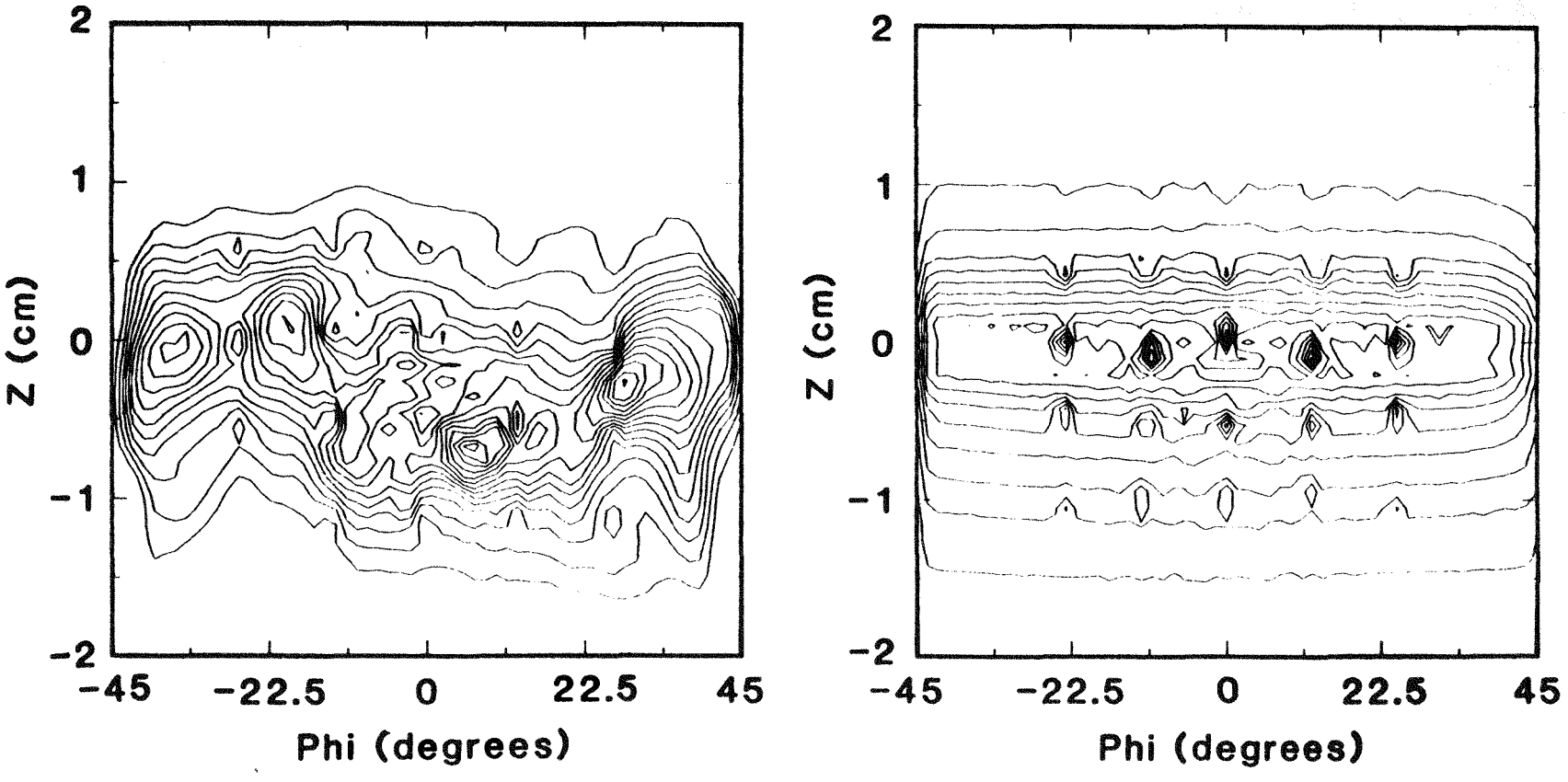
2
1
0
-1
-2
Z (cm)
-45
-22.5
0
22.5
45
Phi (degrees)
2
1
0
-1
-2
Z (cm)
-45
-22.5
0
22.5
45
Phi (degrees)

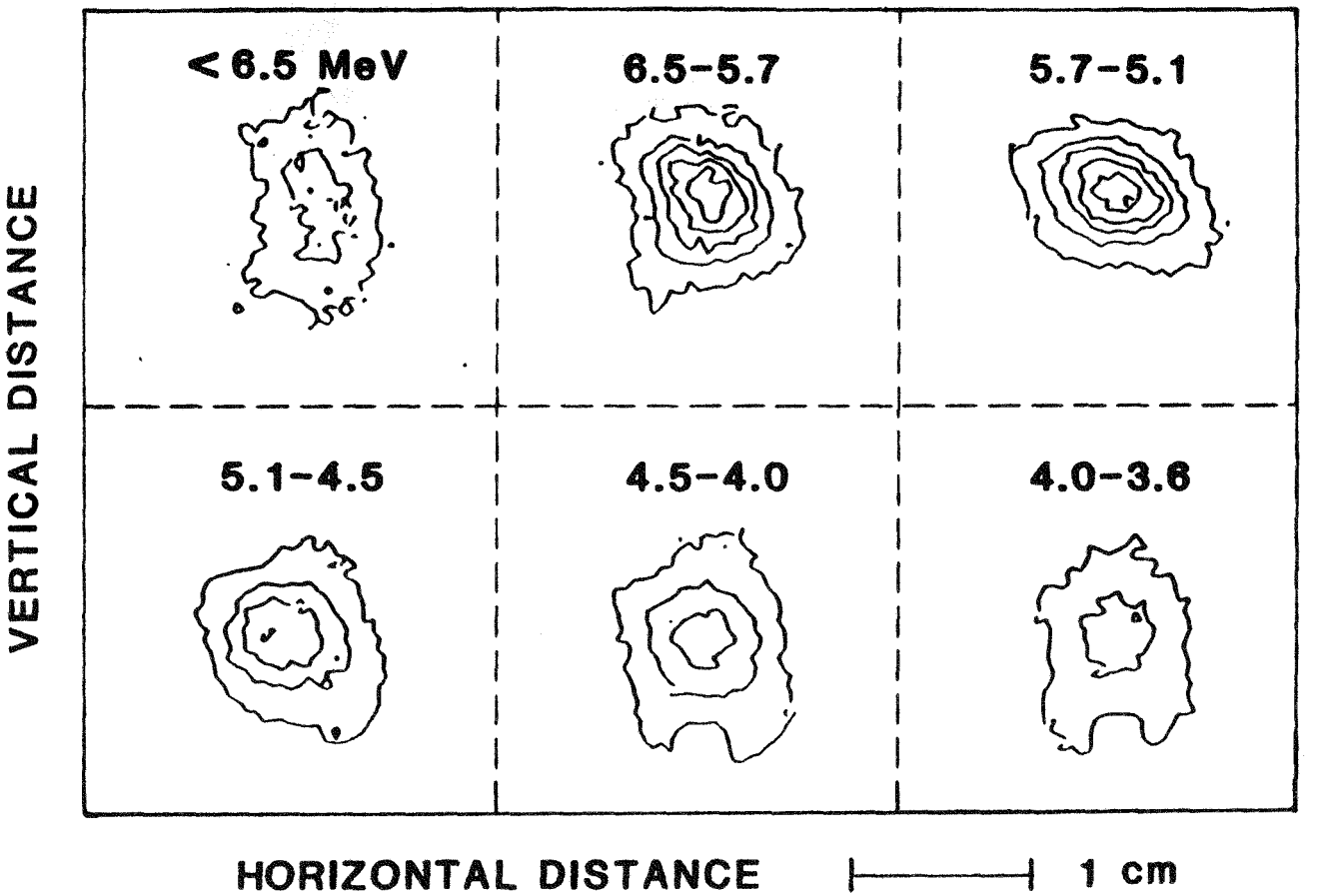
< 6.5 MeV
6.5–5.7
5.7–5.1
5.1–4.5
4.5–4.0
4.0–3.6
VERTICAL DISTANCE
HORIZONTAL DISTANCE
1 cm

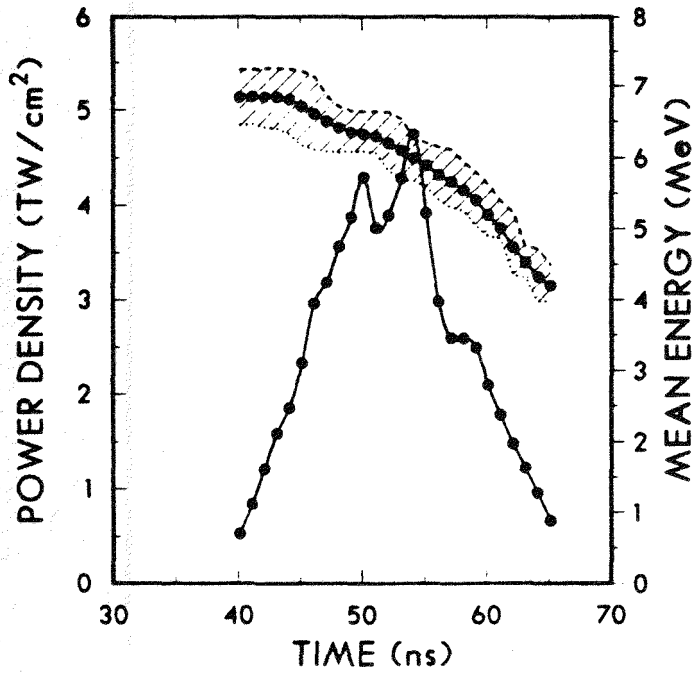
POWER DENSITY (TW/cm²)
MEAN ENERGY (MeV)
TIME (ns)
0
1
2
3
4
5
6
7
8
30
40
50
60
70

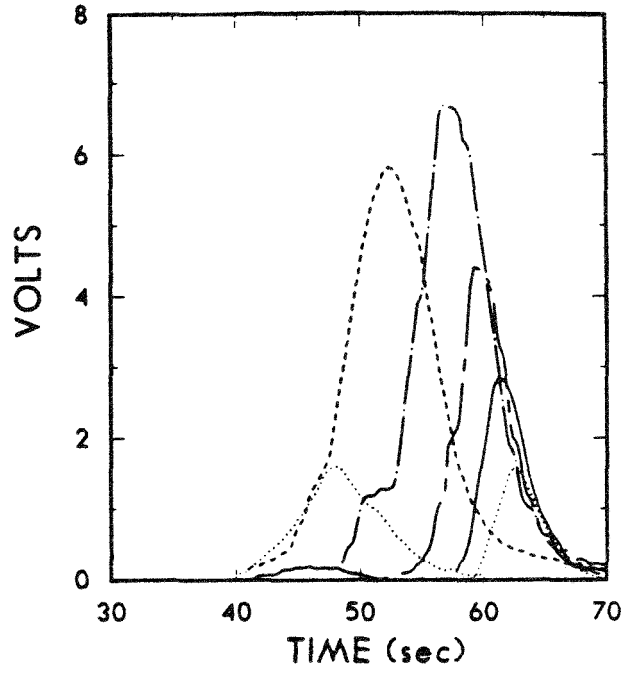
VOLTS
TIME (sec)
0
2
4
6
8
30
40
50
60
70

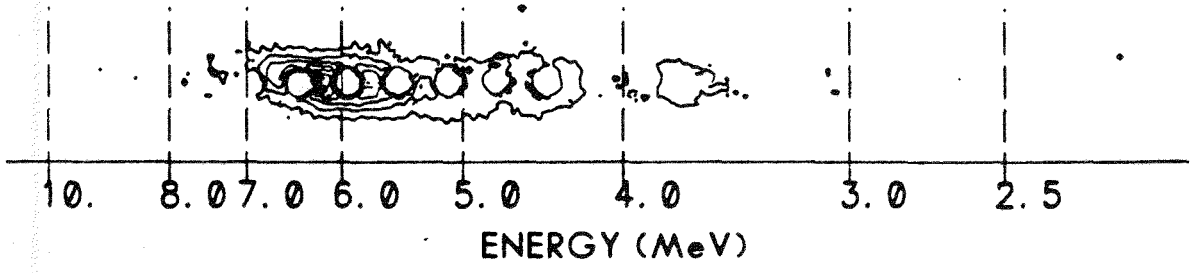
10.
8.0
7.0
6.0
5.0
4.0
3.0
2.5
ENERGY (MeV)